Adaptive beamforming system for radio-frequency interference rejection

M.Goris, A.Joseph, G.Hampson and F.Smits

Abstract: Results from an experimental antenna array that is processed adaptively to cancel external radio-frequency interference are presented. The eight-element array has been tested in a far-field anechoic chamber. The adaptive beamformer rejects sidelobe and main-lobe interference by up to 37 dB. A conventional Fourier beamformer rejects interference only in the sidelobes by between 13 and 30 dB depending on the location of the interference within the array's sidelobes. The adaptive beamformer does not need any *a priori* knowledge about the interfering signals such as the number of interferers or their direction of arrival. The adaptive beamformer also has superior angular resolution to the Fourier beamformer. With an aperture of 4.4 wavelengths and an input signal-to-noise ratio of 37 dB, the adaptive beamformer's resolution is as low as 0.28° while the Fourier beamformer's resolution is 8.8°.

1 Introduction

We report on an adaptive-antenna demonstrator (AAD) system that we developed as part of the 'square kilometre array interferometer' (SKAI) telescope project [1]. The SKAI telescope is being developed in an international effort to produce a next-generation radio telescope with one square kilometre of collecting area. We are researching phased arrays as one way of building SKAI. A phased-array SKAI would be built using around 100 million small antennas operating in a hierarchy of phased arrays [2–5]. The AAD system was built, in part, to provide a platform for developing and testing adaptive array-processing algorithms. It also allows us to investigate the sources and magnitudes of errors in a real array. With these details it will be possible to model arrays more accurately and predict the performance of potential adaptive array algorithms. At this point we have programmed AAD to run a minimum-variance (MV) beamformer [6, 7] and, as a control, a conventional nonadaptive phase-shift-and-sum or Fourier beamformer. Fourier beamforming is the technique used in synthesis imaging [8].

Our effort to develop an adaptive beamformer is a response to the growing problem of radio-frequency interference (RFI). Higher red shift observations are lowering observing frequencies while cheaper RF electronics and increasing consumer demand are taking active RF spectrum users to higher frequencies; RFI will only become worse than it is today. One of the goals of the SKAI telescope is to be able to reject RFI so that we may observe in bands occupied by active users. The techniques that we develop for SKAI may also be applicable to current synthesis telescopes.

IEE Proceedings online no. 19990265
DOI: 10.1049/ip-rsn:19990265

Paper first received 1st May and in revised form 13th October 1998

The authors are with the Netherlands Foundation for Research in Astronomy P.O. Box 2 7990 AA Dwingeloo, The Netherlands
A Joseph is on leave from the RAMAN Research Institute, Bangalore, India

The AAD system has eight patch antennas operating with a bandwidth of 200 MHz at 5.2 GHz. The system's baseband is 4 MHz wide. The array is mounted on a two-axis positioner inside an anechoic room with two far-field signal sources.

Our first results from the AAD system show that we can steer nulls to interfering signals that are both inside and outside the main beam of the array. The MV beamformer rejects interference by up to 37 dB while the Fourier beamformer rejects interference by only 12 to 30 dB, depending on the interference's direction of arrival. The MV beamformer's angular resolution is as low as 0.28° while the Fourier beamformer's resolution is 8.8°.

2 AAD hardware

AAD consists of two transmitters, shown in Fig. 1, and a receiver. The transmitters are in the far field and are about 22° apart when viewed from the position of the array. The first transmitter transmits white noise in an 8 MHz band centred at 5.27 GHz ($\lambda = 5.7$ cm). The second transmitter transmits a continuous wave (CW) signal in the same frequency band.

A diagram of the receiver hardware is shown in Fig. 2. A 2×4 planar-element microstrip antenna array is mounted on a rotating platform, or *positioner*, with two axes of rotation. The spacing between antennas is 1.48λ. The maximum aperture of the array A is therefore 0.252 m. Elements are spaced greater than $\lambda/2$ because of their

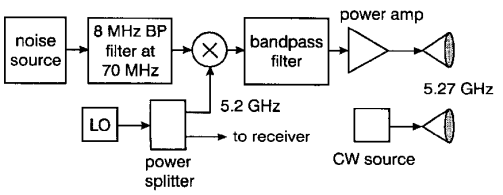

Fig. 1 *Transmitter hardware*

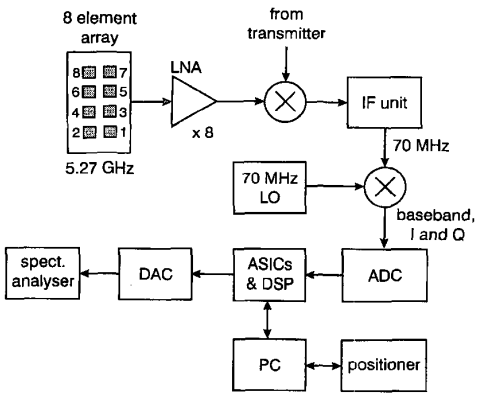

Fig. 2 *Receiver hardware*

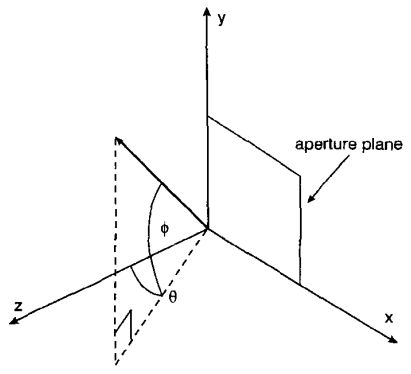

Fig. 3 *Co-ordinate system*
θ = azimuth angle
ϕ = elevation angle

physical size and to minimise mutual coupling. The array's aperture divided by the coherency length is

$$BA/c = 6.7 \times 10^{-3} \ll 1 \quad (1)$$

where c is the speed of light and B is the bandwidth and so the system can be regarded as narrowband and phase changes are equivalent to time delays.

The antenna signals are fed to low-noise amplifiers and then mixed to an intermediate frequency (IF) of 70 MHz. The IF signals are filtered and amplified in the IF unit and fed to a double-sideband quadrature demodulator which mixes the IF signals to baseband. The baseband in-phase (I) and quadrature (Q) signals are filtered using a 7th-order lowpass Chebyshev filter with a 3 dB cut-off frequency of 3.2 MHz. The cut-off frequency is limited by the sampling rate of the digitiser which is 8 MHz; we avoid temporal aliasing by keeping our signal bandwidth less than 4 MHz. The I and Q outputs are digitised to eight bits. The nominal amplitude and phase errors of the quadrature demodulators are 0.2 dB and $\pm 1°$, respectively. We expect that the demodulator errors will create an unwanted image signal although we have not yet measured this experimentally. Gains were set so that the full ADC range was used with minimal ($< 1\%$) clipping.

An adaptive digital beamforming (ADBF) board containing two beamforming ASICs and a Texas Instruments TMS320C30 DSP are responsible for the beamforming. The ASICs, operating in parallel, each multiply four digitised signals with 11-bit complex weights and then together sum all eight channels to give a single 8 MHz 16-bit complex output. The weights are controlled by the DSP which can calculate the weights either adaptively, based on the received signals which are uploaded by the ASICs, or nonadaptively as required. The ADBF board is controlled via a serial link from a PC to the DSP. The PC also controls the positioner and communicates its angular position to the DSP.

3 AAD Software

We briefly introduce our notation and describe the Fourier and MV beamformers. Consider the general case of a two-dimensional array of M antennas where the position of the mth antenna is (x_m, y_m). To simplify equations, all dimensions are normalised by $\lambda/2$. The *steering vector* $\mathbf{a}(\theta, \phi)$ is the response of each antenna to a unit-power signal from direction (θ, ϕ) where θ is in the azimuth direction and ϕ is in the elevation, measured from the normal to the plane of the array (see Fig. 3). The steering vector, or its conjugate, is also known as the gain, the response and the constraint vector. The mth element of $\mathbf{a}(\theta, \phi)$ is

$$a_m(\theta, \phi) = b_m(\theta, \phi) \exp(j\pi(x_m \sin\theta + y_m \cos\theta \sin\phi)) \quad (2)$$

where b_m is a complex scalar with amplitude g_m and phase ψ_m that accounts for the individual antenna responses and the effects of the electronics. The array-covariance matrix (ACM) R is estimated with a time average

$$\hat{\mathbf{R}} = \sum_{k=1}^{K} z(t_k) z(t_k)^H \quad (3)$$

where $z(t_k)$ is a snapshot vector of the antenna outputs, the superscript H represents a hermitian transpose. K is the number of snapshots used to estimate the average and the hat indicates an estimate.

An estimate of the signal that arrives from a given direction $\hat{s}_{(\theta,\phi)}(t)$ and its power $\hat{P}(\theta, \phi)$ are given by

$$\hat{s}_{(\theta,\phi)}(t) = \mathbf{w}^H(\theta, \phi)\mathbf{z}(t) \text{ and} \quad (4)$$

$$\hat{P}(\theta, \phi) = \mathbf{w}^H(\theta, \phi)\mathbf{R}\mathbf{w}(\theta, \phi) \quad (5)$$

where $\mathbf{w}(\theta, \phi)$ is a beamformer weights vector. The mth element of the Fourier beamformer's weights vector $w_F(m)$ with a rectangular window is

$$w_F(m)(\theta, \phi) = \frac{a_m(\theta, \phi)}{M g_m(\theta, \phi)} \quad (6)$$

The MV beamformer weights vector is

$$\mathbf{w}_A = \frac{\mathbf{R}^{-1}\mathbf{a}}{\mathbf{a}^H\mathbf{R}^{-1}\mathbf{a}} \quad (7)$$

In practice we calculate $\mathbf{R}^{-1}\mathbf{a}$ using a Cholesky decomposition.

3.1 Measuring steering vectors

Calibration essentially means measuring the set of all steering vectors called the *array manifold.* The set of all steering vectors is infinite in size and so in practice we measure a finite set of steering vectors on a grid of look directions. We let $\imath_m(\theta, \phi) = \exp(j\pi(x_m \sin\theta + y_m \cos\theta \sin\phi))$ so that $a_m = b_m \imath_m$ and we call $\imath = [\imath_1, \imath_2, \ldots, \imath_M]^T$ the *ideal steering vector* which depends only on the geometry of the array. We know what $\{x_m\}$ and $\{y_m\}$ are and so we can calculate $\imath(\theta, \phi)$ easily (making it ideal). The antenna responses $b_m(\theta, \phi)$ are complicated functions that

cannot be predicted. Our goal is therefore to measure and store in memory the antenna responses. During beamformer operation we use bicubic interpolation [7] to obtain antenna responses off the grid points and then from eqn. 2 recombine them with $\iota(\theta, \phi)$ to give $a(\theta, \phi)$.

The calibration measurements are based on **R**. We assume that the noise is uncorrelated and that there is one signal impinging on the array with nominally unit power and from a known direction (θ, ϕ). In practice, we know the direction to the signal source very accurately because the array is mounted on the positioner which we control. The (jk)th element of the ACM R_{jk} is then given by

$$R_{jk} = a_j a_k^* + \delta_{jk}\sigma_j^2 = (b_j b_k^*)(\iota_j \iota_k^*) + \delta_{jk}\sigma_j^2 \quad (8)$$

where σ_j^2 is the power of the noise at the jth antenna. Knowing $\{\iota_j\}$, we can divide eqn. 8 by $\iota_j \iota_k^*$ and linearise by taking logarithms and then dividing the equation into the real and imaginary parts to give

$$\log\left|\frac{R_j k}{\iota_j \iota_k^*}\right| = \log g_j + \log g_k \;\forall\; k > j \quad (9)$$

$$\angle\frac{R_{jk}}{\iota_j \iota_k^*} = \psi_j - \psi_k \;\forall\; k > j \quad (10)$$

where $\angle$ refers to the phase of a complex number. Eqns. 9 and 10 define over-determined sets of equations because there are $M(M-1)/2$ equations and only M unknowns. Assuming that all $|\psi_j - \psi_k| < \pi$ (*i.e.* there is no phase wrapping), then we solve for $\{g_j\}$ and $\{\psi_j\}$ using linear regression. Because eqn. 10 includes only phase differences there is not a unique solution for the $\{\psi_j\}$. We create a unique solution by assuming that the first sensor of the array is at the origin and that therefore $\psi_1 = 0$.

4 Results

We experimented on the AAD system to determine its performance and to estimate appropriate system parameters.

4.1 Rates of convergence

The aim of this experiment is to know how many snapshots are needed to estimate **R** and, ultimately, steering vectors to a given level of accuracy. We recorded 100 ACMs for certain numbers of snapshots K. The variance of **R** was calculated as the mean of the variance of each element of **R**. We used a single transmitting noise source with constant power. The results in Fig. 4 shows that $\hat{\mathbf{R}}$ converges asymptotically. The plot agrees with the theoretical rate of convergence which is proportional to $1/\sqrt{BK}$ [8]. The steering vector is related linearly to $\hat{\mathbf{R}}$ and so its amplitudes and phases also converge proportionally to $1/\sqrt{BK}$. The exact form of the steering vector convergence will depend on the number of sensors; more sensors will yield more accurate estimates. For AAD the estimation standard deviations are given by

$$\log_{10}(\sigma_{amp}) = -0.48\log_{10}(K) - 0.42$$
$$\log_{10}(\sigma_{phs}) = -0.49\log_{10}(K) + 0.50 \quad (11)$$

where σ_{amp} and σ_{phs} are the standard deviations of the amplitude, as a percentage of the mean antenna response, and phase, in degrees. We found that standard deviations of 4% in amplitude and 3° in phase cause a 1 dB loss in sensitivity of the MV beamformer. Fig. 5 shows the eigenvalues $\{e_m\}$ in descending order when there is one signal source. The input SNR is taken as $(e_1 - e_M)/(Me_M)$ where e_1 and e_M are the largest and smallest eigenvalues, and it equals 28 dB.

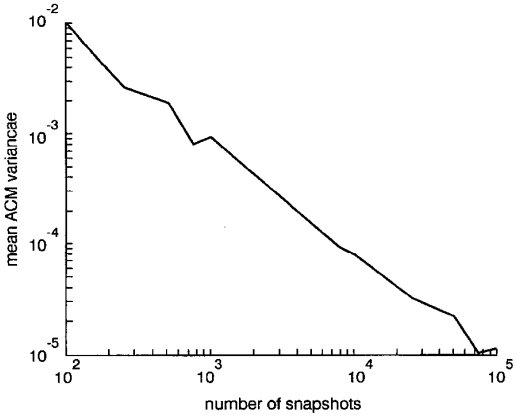

Fig. 4 *Convergence of* $\hat{\mathbf{R}}$

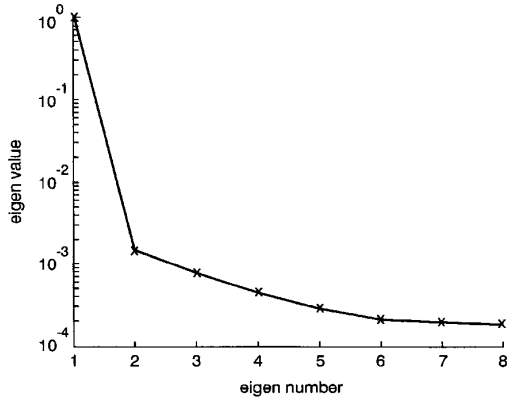

Fig. 5 *Eigenvalues of* **R** *in descending order for one signal source*

Fig. 6 shows the measured phase and amplitude antenna patterns for the second antenna. Note that the phases are measured relative to the phase at the first antenna. The antenna patterns are oscillatory because of mutual coupling between antenna elements as well as coupling between the antennas and the positioner. Bicubic interpolation of the antenna patterns is accurate enough for MV beamforming but a lot of time and memory is required to measure and store the steering vectors on a sufficiently fine grid. We are investigating function approximation and image compression of the antenna responses as an alternative to interpolation to reduce the memory and processing requirements.

4.2 Adaptive nulling capabilities

Fig. 7 shows two radio images of the anechoic room with two signal sources made using the Fourier beamformer and the MV beamformer. The MV beamformer has significantly finer resolution than the Fourier beamformer (down to 0.28° as opposed to 8.8°). The Fourier beamformer has such a large beamwidth in AAD that, with there being two signal sources plus the grating lobes, it is impossible to tell

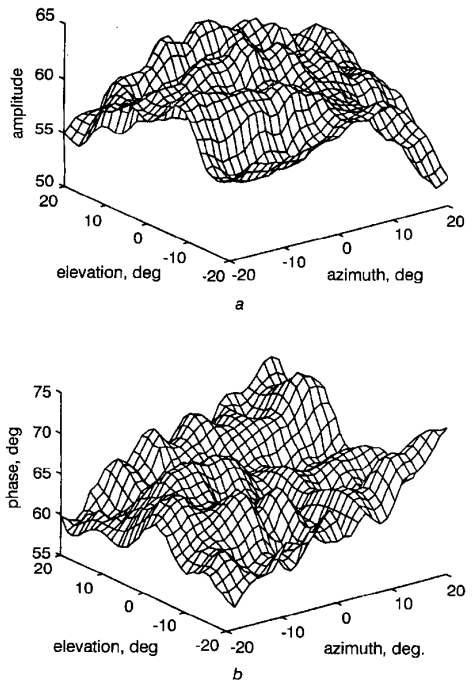

Fig. 6 *Antenna response function, against azimuth θ and elevation ϕ*
a Amplitude
b Phase

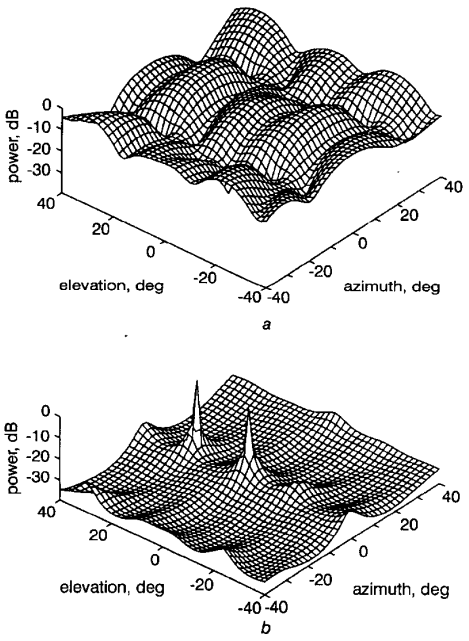

Fig. 7 *Radio images of anechoic room using Fourier and MV beamformers.*
a Fourier
b MV

from the image how many signal sources there really are. The MV beamformer's image clearly shows that there are two signal sources. The MV beamformer's sidelobes are much lower than the Fourier beamformer's (−37 dB as opposed to −12 dB) and they have much less ripple. The Fourier beamformer's sidelobes are very close to the theoretical value of −13 dB for rectangular windows.

Both beamformers have grating lobes whose locations are predicted by

$$\psi_{\text{grating}} = \arcsin\left(\frac{n\lambda}{d} + \sin\theta\right)$$
$$= \pm 43^\circ \text{when } \theta = 0, \text{ and } d = 1.48\lambda \quad (12)$$

where n is an integer. The grating lobes occur because the steering vectors at all $\{\psi_{\text{grating}}\}$ are almost equal. The steering vectors would be equal if the antennas were isotropic. The Fourier beamformer has strong grating lobes because it is insensitive to the small inequalities between the steering vectors at the grating-lobe angles. The MV beamformer has very low grating lobes, at around −20 dB, because it is very sensitive to the steering vector inequalities. They can be seen at the edges of the plot and at (−2°, −17°) in Fig. 7*b*.

4.3 Artificial noise injection

Because we would use the outputs of a number of antenna arrays for synthesis imaging we need stable mainlobe shapes. This means that we cannot allow mainlobe nulling. To reduce the likelihood of mainlobe nulling we can artificially increase the uncorrelated noise power by adding $\sigma^2\mathbf{I}$ to the ACM, where σ^2 is the artificial noise power. There are two side effects of adding artificial noise: the depth of nulls will be reduced and the beam will be wider giving less resolution. Alternatives to the MV beamformer that control the mainlobe shape and which we do not discuss here include the derivative-constrained and norm-bounded beamformers.

We made images of a single source using the MV beamformer with varying amounts of artificial noise. Fig. 8 shows a plot of beam width and sidelobe level against artificial noise power. As we expect, the beam width of the MV beamformer tends to that of the Fourier beamformer with increasing artificial noise. The Fourier beamformer has the least sensitivity to uncorrelated noise and, in the case that uncorrelated noise power far exceeds interference power, the MV beamformer will adaptively choose the same weights as the Fourier beamformer. Interference is suppressed less as artificial noise increases, tending to the −12 dB suppression in the first sidelobe (ideally −13 dB) that the Fourier beamformer with rectangular window gives.

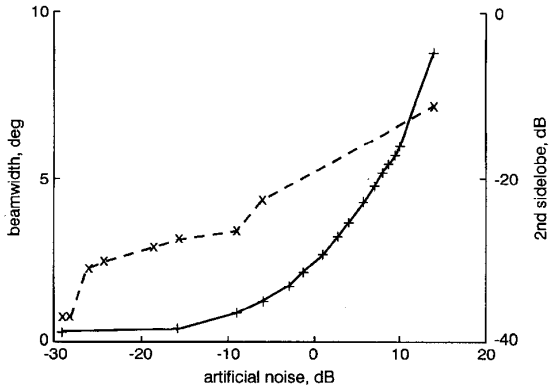

Fig. 8 *MV beamformer's beam width and sidelobe level against artificial noise*
— beamwidth
---- sidelobe level

5 Conclusion

We have built and programmed an eight-element adaptive antenna demonstrator with eight-bit quantisation and using beamforming ASICs and a floating-point DSP. We programmed it to do both Fourier and minimum-variance beamforming. After calibrating the system the MV beamformer nulled interference signals by up to 37 dB. No *a priori* knowledge of the interfering signals is needed. The antenna array has a 2×4 rectangular shape with a distance between antennas of 1.48 wavelengths. The MV beamformer has finer resolution than the Fourier beamformer: as low as 0.28° in the vertical axis compared to 8.8°.

The MV beamformer can null both mainlobe and sidelobe interference. In radio astronomy, we desire to null only signals that are in the side lobes so that the main lobe has a constant or predictable shape. We will be investigating other adaptive beamformers that meet this condition. The MV beamformer has demonstrated the effectiveness of interference nulling. AAD will allow us to investigate other adaptive array algorithms and to investigate their robustness to nonideal hardware and signals.

6 References

1 VAN ARDENNE, A., and SMITS, F: 'Technical aspects of the square kilometer array interferometer.' Proceedings of the ESA workshop on Large antennas in radio astronomy, Noordwijk, The Netherlands, 1996, pp. 117–128

2 SMOLDERS, B.: 'Random sparse arrays, An option for skai?' SKAI memo 034, 1998. Netherlands Foundation for Research in Astronomy. PO Box 2, 7990 AA Dwingeloo, The Netherlands

3 TAN, G.-H.: 'Reliability aspects of a 1 km^2 array'. NFRA note 621, December 1994. Netherlands Foundation for Research in Astronomy, PO Box 2, 7990 AA Dwingeloo, The Netherlands

4 GORIS, M.J.: 'RFI robust algorithms'. Presented at the SKAI technical workshop, December 1997. PO Box 76, Epping 2121, Australia, The Australia Telescope National Facility.

5 JOSEPH, A.: 'RF beamforming techniques for the one square meter array'. SKAI memo 032, 1998. Netherlands Foundation for Research in Astronomy, PO Box 2, 7990 AA Dwingeloo, The Netherlands

6 UNNIKRISHNA PILLAI, S: 'Array signal processing' (Springer-Verlag, 1989)

7 HUDSON, J.E.: 'Adaptive array principles' (Peter Peregrinus Ltd., 1981)

8 KRAUS, J.D.: 'Radio astronomy' (Cygnus-Quasar, 1986, 2nd edn)